Energy Conversion and Management 342 (2025) 120132

Contents lists available at ScienceDirect

Energy Conversion and Management

journal homepage: www.elsevier.com/locate/enconman

Research Paper

Dynamic accounting model with integrated emission allocation methods for coupled energy systems with combined heat and power plants and hybrid heat pumps

Chris Burkel [a,b,c,*], Marco Griesbach [a,c], Florian Heberle [a,c], Dieter Brüggemann [a,c], Andreas Jess [b,c]

[a] Chair of Engineering Thermodynamics and Transport Processes (LTTT), University of Bayreuth, Bayreuth 95440, Germany
[b] Chair of Chemical Engineering (CVT), University of Bayreuth, Bayreuth 95440, Germany
[c] Center of Energy Technology (ZET), University of Bayreuth, Bayreuth 95440, Germany

ARTICLE INFO

Keywords:
Dynamic emission accounting
Quasi-Input-Output (QIO)
Carbon emission flow theory
Emission allocation
Heat pump
Bayreuth method

ABSTRACT

Detailed emission accounting methods are becoming increasingly important as a measurement tool for the decarbonization of energy systems. Conventional accounting methods use only annual demand values and the average grid electricity mix, thereby neglecting dynamic energy and emission flows across the accounting boundary. Moreover, in cases of interconnected supply grids there is a time-dependent exchange of energy and emissions. In this work, a coupled energy system is considered in a dynamic perspective, which connects an electricity, heating and cooling grid through a combined heat and power unit (CHP) and a heat pump (HP) that provides heating and cooling energy at the same time. In order to map the behavior of the emission flows, a dynamic emission balance model is developed using Python. The framework is based on the carbon emission flow theory which is implemented via a Quasi-Input-Output (QIO) node system and uses measured data in an hourly resolution. The dynamic interchange between the grids is enabled by diverse CHP allocation methods that are integrated and applied to the HP. In addition, a method specific for HPs is presented as the Bayreuth method (BaM). The cumulative accounting demonstrates that the allocation methods influence the distribution between the grids, while the resolution determines the absorbed emissions from the public electricity grid. In the case study under consideration, this has the greatest impact on the cooling grid. There is a difference of up to 69 % between the allocation methods and a resolution effect of up to 20 %. The system's overall balance is enhanced by around 10 % due to a higher resolution in comparison with conventional methodologies. It is evident that dynamic balancing models offer a viable solution for accurately capturing the emissions of an energy system. The analysis of temporal emission flows enables seamless tracking and precise accounting results, even beyond the boundary limits. Furthermore, these models can be transferred to other existing systems and provide a framework for the optimization of energy management strategies, facilitating the temporal progression of the emission load.

1. Introduction

The demand for energy such as electricity, heating and cooling in the building sector is still responsible for a large proportion of emissions today. In 2023, around 102 million tons of CO_2 equivalents (CO_2-eq) were emitted in Germany for the operation of buildings, which corresponds to 15 % of Germany's annual emissions [1]. To capture the process of decarbonization, emission accounting is becoming increasingly important as a basis for the measurability of emission reductions. Precision in balancing is directly correlated with the ability to discern minute reductions. However, the variability and complexity of contemporary energy systems lead to an ever more intricate allocation of emissions.

The growing mix of centralized and decentralized energy supply results in a multifaceted energy landscape, characterized by a complex interplay of diverse energy flows, each with distinct emission profiles [2]. This complicates the tracking of emissions across the balance boundaries and allocating them to individual consumers. Consequently, the conventional approach of assessing the emission balance by only

* Corresponding author at: Chair of Engineering Thermodynamics and Transport Processes (LTTT), University of Bayreuth, Bayreuth 95440, Germany.
E-mail address: chris.burkel@uni-bayreuth.de (C. Burkel).

https://doi.org/10.1016/j.enconman.2025.120132
Received 24 March 2025; Received in revised form 23 June 2025; Accepted 26 June 2025
Available online 30 June 2025

Nomenclature

Abbreviations

AC	absorption chiller
BaM	Bayreuth method
CC	compression chiller
CD	cooling demand
CHP	combined heat and power
CO_2-eq	CO_2-equivalents
ED	electricity demand
ENTSOE-E	European network of transmission system operators for electricity
EnM	energy method
EfM	efficiency method
ExM	exergy method
FC	free cooling
GB	gas boiler
HD	heating demand
HES	heat energy storage
HP	heat pump
IES	ice energy storage
IPCC	Intergovernmental panel on climate change
MN	merging node
QIO	quasi-input–output
TAO	Technology alliance upper Franconia
TI	transformer input
TO	transformer output

Symbols

C	energy status storage (kWh)
COP	coefficient of performance (−)
$corr$	correction factor (−)
E	emissions (kg)
EER	energy efficiency ratio (−)
e	specific emissions (kg/kWh)
H	number of time steps (−)
p	proportion of input flows (−)
r	allocation ratio (−)
S	total quantity of measured values (−)
s	measured value (−)
T	temperature (K)
t	time step (−)
W	energy (kWh)

Greek symbols

η	efficiency (−)

Subscripts and superscripts

C	Carnot
$corr$	correction
el	electricity
exe	external exergetic
exi	internal exergetic
i	source
in	input
j	node number
k	sink
m	mean
min	minimum
out	output
$prim$	primary side
sec	secondary side
th	thermal

considering the summed input flows, as if the system were a black box, is no longer adequate in many cases. To address this, it is important to consider the energy flows, including their temporal emission dependence, resulting from internal system combinations and purchased energy from the public grid.

Before a system can be analyzed in more detail within its accounting boundaries, it is necessary to know which emissions are absorbed by the supply from the public grid. The temporal dependency of the electricity grid is a salient factor in this regard, and this dependency is further reinforced by the expansion of renewable energies [3]. When applied to the domain of emissions accounting, this implies that the temporal influence on the emission load also increases. Transferred to a building that also represents the balance boundary and draws electricity from the public grid, the emission absorption is time and quantity dependent.

For this reason, more and more researchers have used the carbon emission flow theory in recent years, see [4–8]. With the help of this theory, it is possible to consider variable input emission loads and to track these with a coupled energy flow through an entire grid system. Tranberg et al. [9] have developed a method that calculates the emission load of the European electricity grids and links them via a node system. This approach enables the analysis of both the current electricity generation in individual countries and the electricity trade occurring simultaneously. For example, this results with an hourly analysis in an annual maximum of 684 g CO_2-eq/kWh and an annual minimum of 92 g CO_2-eq/kWh for Germany in 2023 [10]. When these dynamics are applied to an emissions balance, discrepancies arise in comparison to conventional methods, such as the Greenhouse Gas Protocol, which operates with annual average values [11].

Bontekoe et al. [12] compare two residential complexes that are in different stages of renovation, insulation and usage of renewable energies. Furthermore, the energy mix of the public grid utilized is derived from Netherlands, Sweden and France. As a result, this research demonstrates the impact of country-specific emission factors and calls into question the common annual perspective by way of a comparison with hourly values. He et al. [13] analyzed a case study consisting of an electricity grid in which a fossil and a renewable share are fed and various load profiles are drawn. From this, a Quasi-Input-Output (QIO) node model was created to determine a dynamic emission factor. The comparison with a static emission factor revealed a significant difference between the totalled emission quantities. In the period under review, the two methods differ by 75 %. Roux et al. [14] could also demonstrate this effect using the example of an energy-efficient house that draws electricity from the public grid in France. Here too, the use of the annual average mix leads to an underestimation of greenhouse gas emissions by 36 %. Álvares Flórez et al. [15] use the aggregated electricity consumption profile of 226 real households and compare the emission balances with constant annual and hourly factors. The two strategies also show a significant discrepancy of 50 %.

If the system is afterwards considered within the balance boundary, the electricity consumed, including emissions, can be converted into alternative forms or mixed with additional energy flows. This is demonstrated by Chicco et al. [16] and Mancarella et al. [17]. An interesting case in this context is CHP generation. In CHP systems, two energy flows are provided from one source. This is also associated with the distribution of the resulting emissions. For this reason, a variety of approaches have been developed in recent years to enable an allocation to the energy flows. Basically, these methods can be divided into two categories. The methods of the first category relate only to the parameters and efficiency of the system under consideration, while the methods in the second category include a comparison of reference

systems with a single energy output. While Buchenau et al. [18] and Rosen [19] have compiled a detailed overview and comparison of these methods, Noussan et al. [20] have carried out the allocations for various system configurations. Furthermore, Holmberg et al. [21] were able to evaluate that the methodologies are applicable to real systems and observed significant differences in the distribution of emissions between electricity and thermal energy.

In order to be able to consider this distribution in an overall system with several interconnected components, Cheng et al. [22] combine the carbon emission flow theory with the allocation methods of the CHP units. In the present context, the energy method is used for CHP allocation, which makes it possible to distribute and track emissions in a multiple energy system. In contrast, Yang et al. [23] consider the overall system from an exergetic perspective and therefore use an exergetic method for the emission allocation of the integrated CHP. While these CHP methods are already being used in a wide variety of studies, there are still no specific methods known for other systems that also generate two output streams from one energy source, like hybrid operated HPs.

The aim of this work is to develop a dynamic QIO model using the emission flow theory for a case study based on real measured values in an hourly resolution for the year 2023. The case study under consideration is a research building at the University of Bayreuth which has its own energy generation system with electricity, heating and cooling supply. The building envelope is therefore the balance boundary and the emission flows of input and output are the subject of the treatment. As a distinctive feature for the emission accounting, the system has a CHP unit and a hybrid operated HP coupled with an ice energy storage (IES). These components create a connection between the three supply grids and thus an exchange of energy and emissions. In contrast to extant models in the literature, the present study analyzes the exchange between the electricity grid and two thermal grids. Furthermore, the dynamic emissions absorbed by the public grid are to be tracked beyond the balance boundary and distributed to the individual grids until the demand side. In this context, the influence of different resolutions of this drawn emission load is to be analyzed and compared to the common annual accounting strategy. As the distribution between the grids depends on the allocation method, different methods have to be considered for the CHP unit and the HP. By referring to the measured values, it also gives the allocation a dynamic behavior. As previously mentioned, there is no detailed observation of emission allocation methods for hybrid HPs in the literature. To address this knowledge gap and enable allocation for HPs as well, it is necessary to transfer and test the already known CHP methods. In line with these insights, a specific method for HPs is also being developed and tested on the case study. In addition to the supply components, the emission flows are even influenced by energy storage systems. These decouple the emission loads from the energy flow in a temporal balance. In other words, the emission load released when the storage is discharged depends on how the storage was previously charged. These influences should therefore also be included in the dynamic balancing model.

2. Description of the case study

This chapter provides a detailed description of the case study examined. Initially, the energy supply system is the primary focus, followed by a comprehensive description of the measurement data obtained from it. Finally, the site-specific and time-dependent energy mix is described in more detail as a further important component of the subsequent emissions balance.

2.1. Description of the system

The Technology Alliance Upper Franconia (TAO) building is located on the campus of the University of Bayreuth. This research building covers a total floor area of 5,600 m^2, of which 4,000 m^2 are used for laboratories and workshops. In contrast to the other buildings of the university, which are supplied via a central energy system, the TAO building is equipped with its own decentralized energy system. This system consists of three energy grids that supply the building with heating, cooling and electricity. The configuration of the primary components and the associated energy flows are illustrated in Fig. 1 as a Sankey diagram.

A distinctive aspect of this research building is the 500 m^3 ice energy storage (IES). This system combines a brine-to-water heat pump that utilizes the ice storage tank as a heat source and can therefore provide cooling energy and store it over a longer time horizon. The residual heat requirement is covered by a CHP unit and a gas boiler (GB) in conjunction with a heat energy storage (HES). For the cooling grid, the additional demand is provided by a compression chiller (CC), an absorption chiller (AC) and a re-cooling unit of the CC as free cooling (FC) at low ambient temperatures. A comprehensive description, including all nominal capacities, can be found in previous publications, see Griesbach et al. [24,25].

2.2. Measurement data and load profiles

The energy requirements of the building are analyzed for the year 2023 and comprise 1,481 MWh of electricity, 771 MWh of heating and 413 MWh of cooling. The primary cause of the heat requirement is space heating, while the cooling energy is in addition to space cooling used for cooling machines via the laboratory cooling grid. This means that the cooling requirement depends very individually on research operations and the academic year. Consequently, demand remains relatively stable, and no clear annual temperature dependency can be discerned. To avoid double counting in the energy balance, electricity demand (ED) is only allocated to the consumption side. This also includes the requirements for the distribution of energy grids, such as pumps and ventilations systems. The proportions converted into thermal energy and used for the provision of heating demand (HD) and cooling demand (CD) are not included in the ED here. The annual load profiles of the three grids are shown in Fig. 2.

The shares of the various supply systems in the load profiles are crucial for the further calculations. In addition to the energy input and output values, some temperature levels must also be considered for exergetic emission allocation methods. Table 1 lists all recorded data for the existing utility system. The measurement intervals and accuracies can also be taken from the previously published works by Griesbach et al. [24,25]. In this study, the recorded energy data is transformed into hourly load values. While most of the data can be recorded by the measuring systems, there are some data points that must be estimated within the accounting model. To obtain the input and output energy flows of the HES, the difference between the heat generated and the HD is utilized. The ED on the consumer side is determined similarly. Here, a balance is applied that considers the electricity purchased with the transformer input (TI), the electricity supplied with the transformer output (TO), the electricity generated with the CHP and the demand for thermal energy generation.

The ambient temperature is also required in the model, so the hourly records from the weather station of the university are used [26].

2.3. Emissions of grid-sourced electricity

The energy sources, including their emission loads, are decisive for the emissions balance. In particular, the emission load of electricity from the public grid exhibits significant fluctuations. As demonstrated in Fig. 3, a sample summer week in 2023 is selected to illustrate the German electricity generation, import/export behavior and grid load. Due to the weather dependency of renewable electricity generation and the fluctuating national electricity demand, the ratio of renewable to fossil electricity generation constantly changes. Furthermore, electricity trade with neighboring countries is a constant occurrence. Consequently, the emissions impact of the electricity drawn from the public

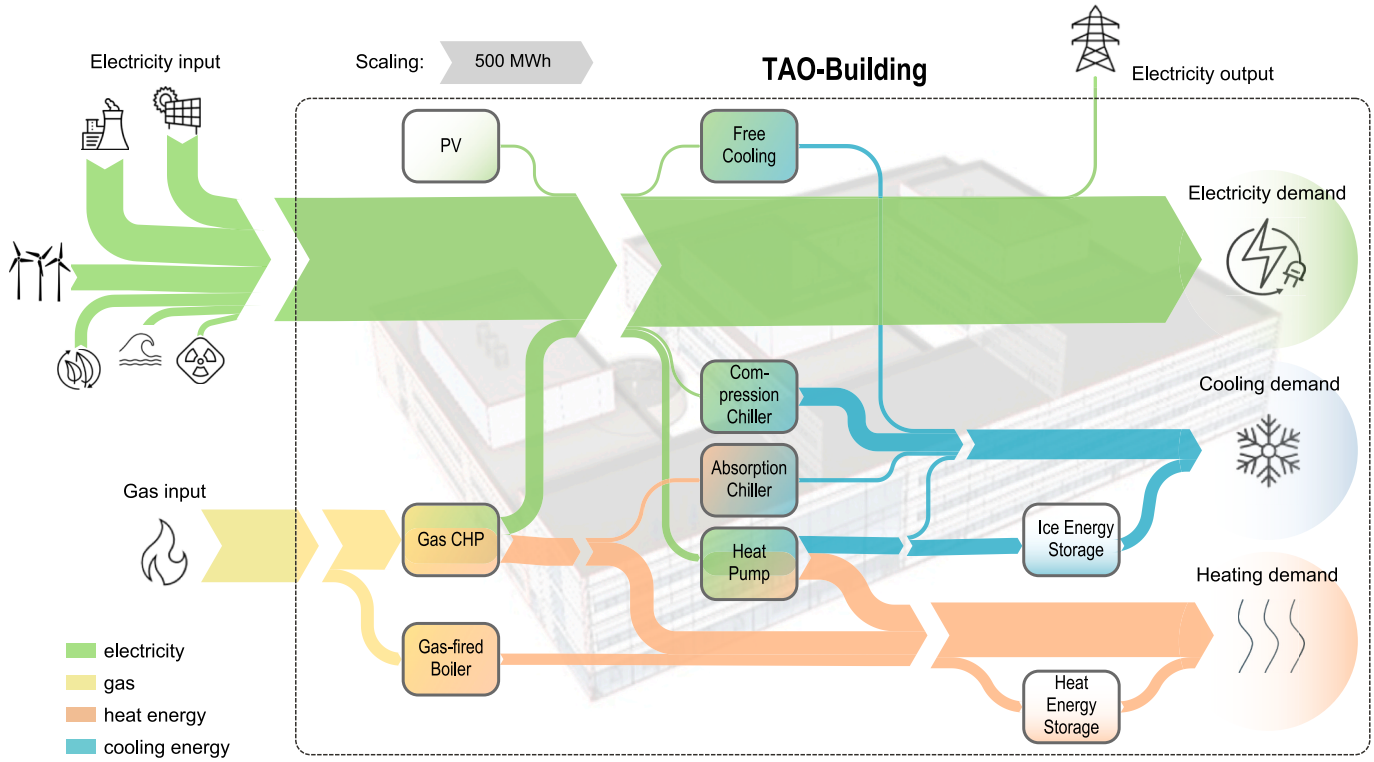

Fig. 1. The primary components of the energy system of the TAO building with the proportional energy flows of the year 2023 and the balance boundary as a Sankey diagram.

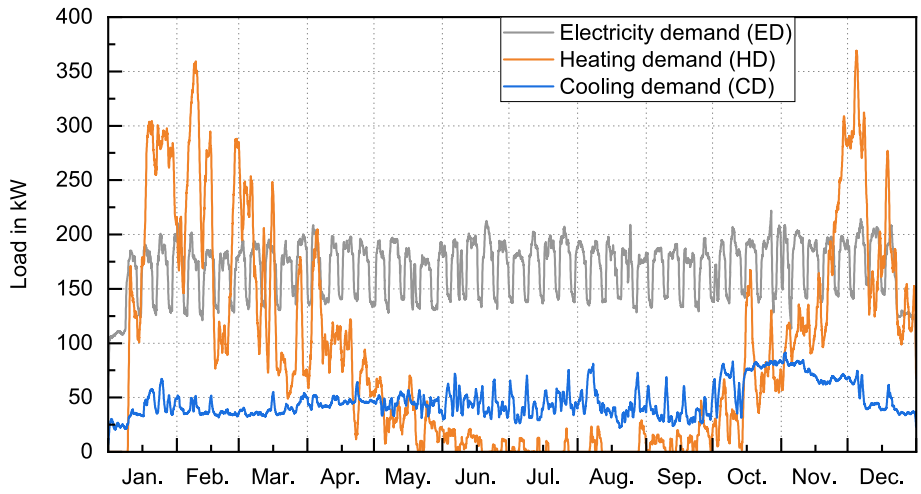

Fig. 2. Load profiles in an hourly resolution of the TAO buildings supply grids for the year 2023: electricity demand (ED), heating demand (HD) and cooling demand (CD).

grid is influenced not only by the share of generation, but also by the share of imports and exports. For comparison, an example winter week in 2023 is shown in the Appendix, see Fig. 19. This shows a higher average residual load, which fluctuates less strongly due to the lower influence of renewable energies.

The methodology of Tranberg et al. [9], which has already been described in the introduction, is also used by the Electricity Maps platform [10]. The data utilized for this mainly arises from the European Network of Transmission System Operators for Electricity (ENTSO-E) [28]. The conversion into specific emission loads is based on data from the Fifth Assessment Report of the Intergovernmental Panel on Climate Change (IPCC) [29]. The resulting emission loads are stated in g CO_2-eq/kWh, i.e. the global warming potential of all greenhouse gases emitted is converted into equivalents in relation to the global warming potential of CO_2. In conjunction with this methodology, the calculated values are made available in various resolutions via Electricity Maps [10], see Fig. 4. The courses of the sample weeks are shown in Fig. 20 and Fig. 21 in the Appendix.

3. Methodology

The energy system of the TAO building is modelled as a nodal system in order to capture the characteristics and relationships between the system components in a computational model. This enables continuous monitoring of externally supplied energy and emissions throughout the entire system. The model shown in Fig. 5 is implemented as a Python

Table 1
Overview of the measurement data utilized in the accounting model.

Component	Value	Unit	Comment
CHP	heat	kWh	–
	electricity	kWh	–
	gas	m^3	volume at standard condition
	temperatures	°C	–
HP	heat	kWh	–
	cold	kWh	–
	electricity	kWh	–
	temperatures	°C	–
GB	heat	kWh	–
	gas	m^3	volume at standard condition
FC	cold	kWh	–
	electricity	kWh	manufacturer data
CC	cold	kWh	–
	electricity	kWh	
AC	heat	kWh	2023 not in operation
	cold	kWh	
IES	cold input	kWh	–
	cold output	kWh	–
HES	heat input	kWh	calculated
	heat output	kWh	calculated
TI	electricity	kWh	–
TO	electricity	kWh	–
ED	electricity	kWh	calculated
HD	heat	kWh	–
CD	cold	kWh	–

code in the Spyder environment [30] and contains various types of nodes. In addition to the system components, which are based on measured values, merging nodes (MN) are used to couple different emission flows with each other.

Furthermore, input and output nodes are used to feed energy and emissions into the system and out of it. In this way, the energy grid can be analyzed in an hourly resolution and the sum of the emission values can be used to create a detailed annual emissions balance. As mentioned in chapter 2.2, it should be noted that this model considers only the main energy flows. Others, such as the electricity for system control, are addressed through the demand of the electricity grid. The boundary conditions and the calculation methods for the different node types are described in the following chapters.

3.1. Emission tracking

To ensure comparability between the different areas, all emission values are calculated as specific values. The emission load e can be determined by the emissions E transported by the energy W:

$$e = \frac{E}{W} \tag{1}$$

The interaction between the nodes is defined by their inflows and outflows. With the measured energy flows, it is possible to calculate the emission load at each node j for each time step t. In relation to node j, the

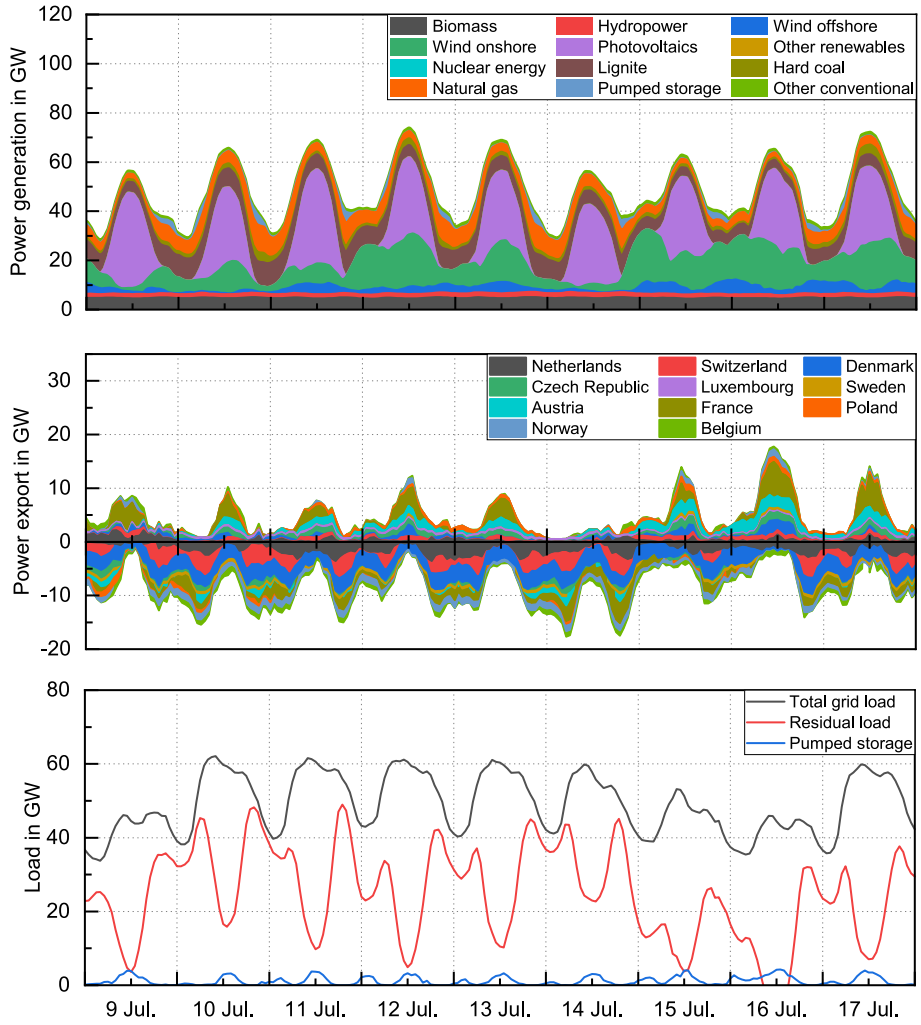

Fig. 3. Example summer week in 2023 of the German electricity production, the import/export behavior and the national electricity demand based on the data from SMARD [27].

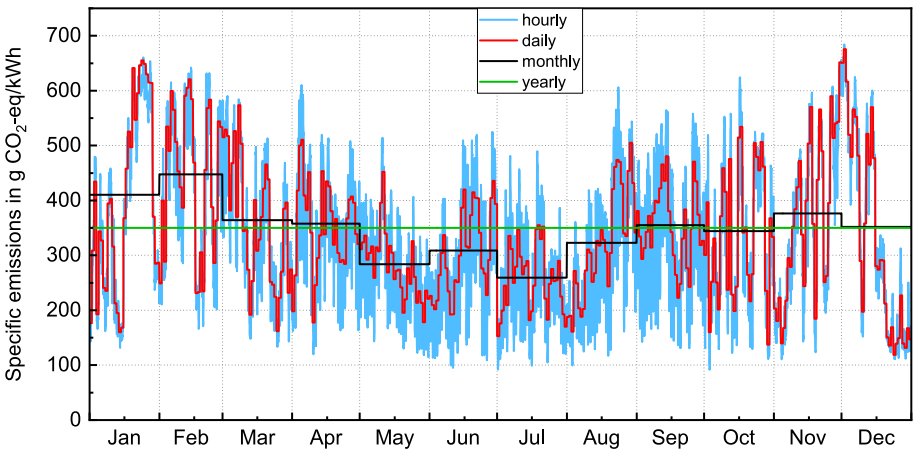

Fig. 4. Different resolutions of the emission load of the German public electricity grid for the year 2023 based on the data from Electricity Maps [10].

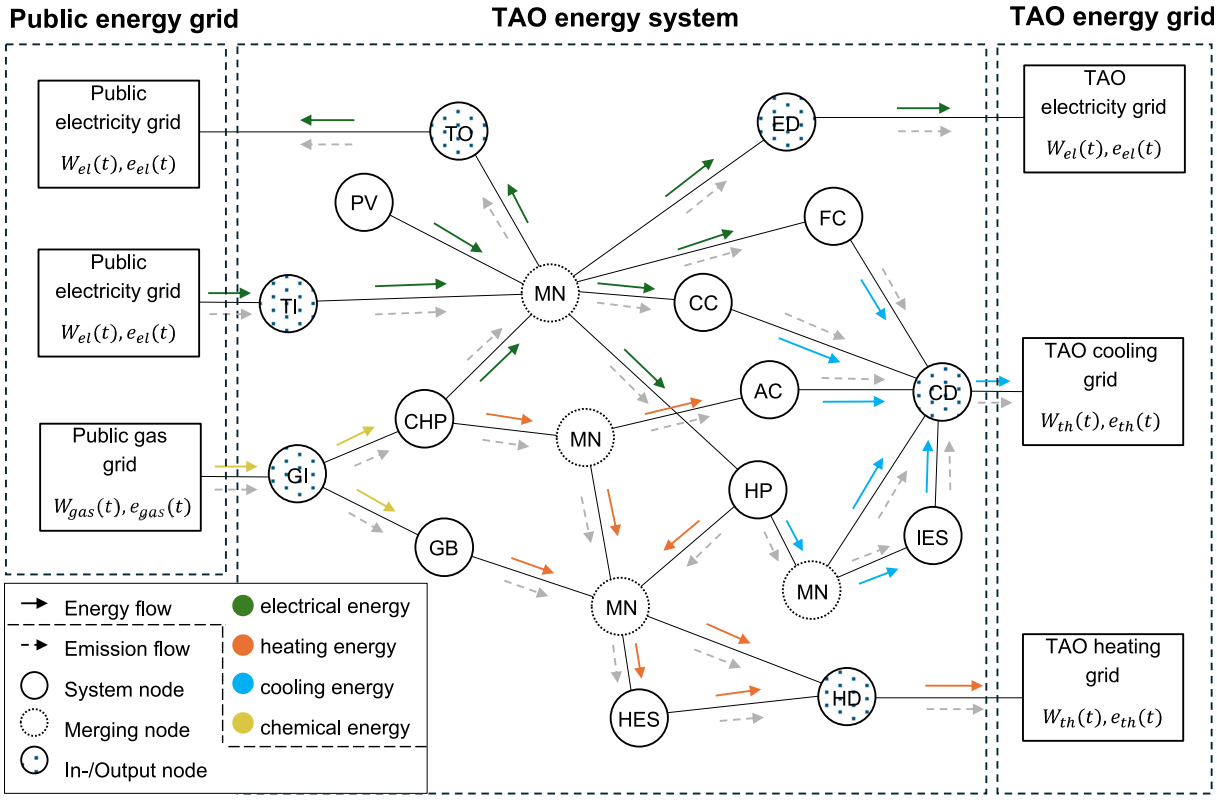

Fig. 5. Visualization of the flow logic for the computational node model.

nodes i represent the sources and the nodes k the sinks. This conceptual model is illustrated in Fig. 6.

Given that the measured data are available in an hourly resolution, the number of time steps for the year under consideration is $H = 8760$. In this instance, the number of sources and sinks for the considered node is clearly defined by examining the specific system.

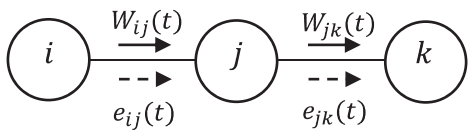

$$i_1, i_2, i_3, \ldots, i_n = sources \qquad k_1, k_2, k_3, \ldots, k_n = sinks$$

Fig. 6. Quasi input–output node model for considering the energy and emission flow.

To mitigate the impact of measurement uncertainties, such as negative energy flows, only values greater than or equal to zero are considered in the analysis. The total quantity of all measured values S consists of real numbers s:

$$S = \{s \in \mathbb{R} | s \geq 0\} \tag{2}$$

3.2. Input and output nodes

The input and output nodes act as sources and sinks for the entire system, see Fig. 5. In this case, the sources are the procurement of electricity (TI) and natural gas (GI) from the public grid. Conversely, the sinks comprise the energy demands of the supply grids (ED, HD and CD)

and the return of electricity (TO) to the public grid. The initial emission flows are defined through the linkage of measured energy input values with specific emissions. For the electrical input, the values of Electricity Maps [10] are used in the desired resolution. The purchased gas volume flow is converted into an energetic flow with the help of monthly calorific values published by the local energy supplier [31]. The combustion of this natural gas yields a specific emission value of 202 g CO_2-eq/kWh into the system [18,20]. As a result, in this case study direct emissions and those resulting from the generation of the purchased electricity are considered. According to the Greenhouse Gas Protocol, these are designated as Scope 1 and Scope 2 emissions [11]. This means that the electricity generated by the internal PV system does not contribute any emissions of this kind to the energy system.

3.3. Merging nodes

The three supply grids are fed by different generation plants. The resultant energy flows and emission loads are interconnected. To account for this mixing, nodes are defined that calculate a time-dependent specific emission factor from the feed-ins. The initial step involves calculating the sum $W_{in,j}(t)$ of the input flows:

$$W_{in,j}(t) = \sum_i W_{ij}(t) \tag{3}$$

The proportions of the input flows $p_{ij}(t)$ are determined in order to establish a correlation between the input flows and their respective counterparts:

$$p_{ij}(t) = \frac{W_{ij}(t)}{W_{in,j}(t)} \tag{4}$$

The specific output emissions $e_{jk}(t)$ of the node j can now be calculated from the sum of the proportional emission loads:

$$e_{jk}(t) = \sum_i p_{ij}(t) e_{ij}(t) \tag{5}$$

3.4. System node: single input/single output

In the context of system nodes, the efficiency $\eta_j(t)$ can be determined for each time step. This is achieved by utilizing the measured values at the input $W_{in,j}(t)$ and output $W_{out,j}(t)$:

$$\eta_j(t) = \frac{W_{out,j}(t)}{W_{in,j}(t)} \tag{6}$$

The output emission load $e_{out,j}(t)$ is contingent on the calculated efficiency and the input emission load $e_{in,j}(t)$:

$$e_{out,j}(t) = \frac{e_{in,j}(t)}{\eta_j(t)} \tag{7}$$

3.5. System node: CHP allocation methods

To ensure transferability between CHPs and hybrid HPs, it is imperative to utilize allocation methods of category 1 exclusively. These methods are confined to the system under consideration, precluding the necessity for comparisons with reference systems. Consequently, the energy method (EnM), efficiency method (EfM), and exergy method (ExM) are employed in this study.

3.5.1. Energy method

The allocation of the emission loads in accordance with the EnM is based on the efficiency of the output energies. Using the measured data, it is feasible to calculate the electrical efficiency $\eta_{el,j}(t)$ and thermal efficiency $\eta_{th,j}(t)$:

$$\eta_{el,j}(t) = \frac{W_{out,el,j}(t)}{W_{in,j}(t)} \tag{8}$$

$$\eta_{th,j}(t) = \frac{W_{out,th,j}(t)}{W_{in,j}(t)} \tag{9}$$

These parameters are now set in relation to the total efficiency of the CHP plant. This enables the division of emissions into electrical components $e_{el,j}(t)$ and thermal components $e_{th,j}(t)$ [18]:

$$e_{el,j}(t) = \frac{e_{in,j}(t)\frac{\eta_{el,j}(t)}{\eta_{el,j}(t)+\eta_{th,j}(t)} W_{in,j}(t)}{W_{out,el,j}(t)} \tag{10}$$

$$e_{th,j}(t) = \frac{e_{in,j}(t)\frac{\eta_{th,j}(t)}{\eta_{el,j}(t)+\eta_{th,j}(t)} W_{in,j}(t)}{W_{out,th,j}(t)} \tag{11}$$

3.5.2. Efficiency method

The EfM does not merely compare the two energy flows with the total efficiency. Furthermore, the two partial efficiencies of the output flows influence each other [18]:

$$e_{el,j}(t) = \frac{e_{in,j}(t)\frac{\eta_{th,j}(t)}{\eta_{el,j}(t)+\eta_{th,j}(t)} W_{in,j}(t)}{W_{out,el,j}(t)} \tag{12}$$

$$e_{th,j}(t) = \frac{e_{in,j}(t)\frac{\eta_{el,j}(t)}{\eta_{el,j}(t)+\eta_{th,j}(t)} W_{in,j}(t)}{W_{out,th,j}(t)} \tag{13}$$

As illustrated in Fig. 7, the two methods are demonstrated as allocation factors across a selected efficiency range. This means that the displayed value can be multiplied by the input emission flow to derive the partial emission flows. It is evident that the EnM (green) depends only on the total efficiency. The EfM (orange/blue), on the other hand, shows the interactions between the partial efficiencies. For a better understanding, an example point with an electrical efficiency of 50 % and a thermal efficiency of 40 % is marked (red). Assuming a CHP plant that releases an input emission load of 100 g CO_2-eq/kWh, the quantity can be divided up using the emission factors shown. If the EfM is selected, approx. 138 g CO_2-eq/kWh are allocated to the thermal energy and approx. 90 g CO_2-eq/kWh to the electrical energy. With EnM, the allocation is the same for both sides and amounts to approx. 111 g CO_2-eq/

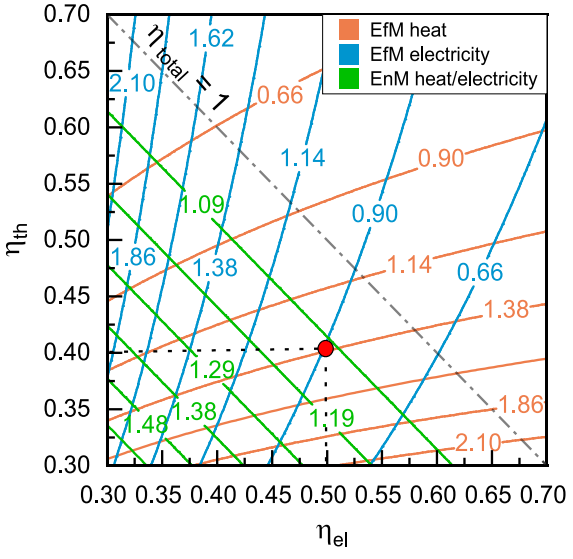

Fig. 7. Illustration of the allocation factors of the energy method (EnM) and efficiency method (EfM) for CHP.

kWh.

3.5.3. Exergy method

The ExM differs from the previously presented methods. It considers the exergy content of the output energies. Assuming the exergetic efficiency of the electrical energy to be 100 %, the determination of the exergy content is confined to the thermal energy. To this end, the mean logarithmic temperature $T_{m,j}(t)$ of the flow temperature $T_{out,j}(t)$ and return temperature $T_{in,j}(t)$ is calculated first:

$$T_{m,j}(t) = \frac{T_{out,j}(t) - T_{in,j}(t)}{\ln \frac{T_{out,j}(t)}{T_{in,j}(t)}} \tag{14}$$

The Carnot efficiency $\eta_{c,j}(t)$ can be determined through a comparison with the ambient temperature $T_a(t)$, which is also available in hourly values:

$$\eta_{c,j}(t) = 1 - \frac{T_a(t)}{T_{m,j}(t)} \tag{15}$$

The obtained Carnot factor can be used to describe the usable proportion of thermal energy. Analogous to the EnM, it is considered as a further influencing factor for the allocation of the two partial emission flows [18]:

$$e_{el,j}(t) = \frac{e_{in,j}(t)\frac{\eta_{el,j}(t)}{\eta_{el,j}(t)+\eta_{c,j}(t)\eta_{th,j}(t)}W_{in,j}(t)}{W_{out,el,j}(t)} \tag{16}$$

$$e_{th,j}(t) = \frac{e_{in,j}(t)\frac{\eta_{c,j}(t)\eta_{th,j}(t)}{\eta_{el,j}(t)+\eta_{c,j}(t)\eta_{th,j}(t)}W_{in,j}(t)}{W_{out,th,j}(t)} \tag{17}$$

This methodology can also be represented as a diagram, see Fig. 8. This time, the allocation factor depends on three variables, so the diagram is divided into two sections: the allocation factor for electricity (left) and the allocation factor for heat (right). It can be seen that as Carnot efficiency decreases, the allocation of emissions becomes more dependent on thermal efficiency.

3.6. System node: Transfer of the allocation methods to heat pumps

After the selection and description of suitable CHP allocation methods, the three methods from chapter 3.5 are transferred and adapted to HPs in the following.

3.6.1. Energy method

As with the EnM for CHP systems, the energy input is also compared with the output energies to determine the efficiency of the HP. The difference here is that there are two thermal output energies. As it is usual with HPs, heat is supplied on the secondary side $W_{out,sec,j}(t)$ and cooling is supplied on the primary side $W_{out,prim,j}(t)$. This results in a coefficient of performance for the heat $COP_j(t)$ and an energy efficiency ratio for cooling $EER_j(t)$:

$$COP_j(t) = \frac{W_{out,sec,j}(t)}{W_{in,j}(t)} \tag{18}$$

$$EER_j(t) = \frac{W_{out,prim,j}(t)}{W_{in,j}(t)} \tag{19}$$

Subsequent to the insertion of these values into equations (10) and (11), according to [18], the ensuing emission distribution is obtained:

$$e_{sec,j}(t) = \frac{e_{in,j}(t)\frac{COP_j(t)}{COP_j(t)+EER_j(t)}W_{in,j}(t)}{W_{out,sec,j}(t)} \tag{20}$$

$$e_{prim,j}(t) = \frac{e_{in,j}(t)\frac{EER_j(t)}{COP_j(t)+EER_j(t)}W_{in,j}(t)}{W_{out,prim,j}(t)} \tag{21}$$

3.6.2. Efficiency method

The same can be adopted in the context of the EfM. In this context too, the equations (12) and (13), which are based on [18], are specified for HPs:

$$e_{sec,j}(t) = \frac{e_{in,j}(t)\frac{EER_j(t)}{COP_j(t)+EER_j(t)}W_{in,j}(t)}{W_{out,sec,j}(t)} \tag{22}$$

$$e_{prim,j}(t) = \frac{e_{in,j}(t)\frac{COP_j(t)}{COP_j(t)+EER_j(t)}W_{in,j}(t)}{W_{out,prim,j}(t)} \tag{23}$$

The allocation factors of these methods are shown in Fig. 9. A comparison of the allocation behavior between Fig. 8 and Fig. 9 indicates that the allocation factors are significantly lower than for the CHP system. This is due to the transformation of the calculation with efficiencies to a calculation with performance factors. If the input emissions are balanced with the output emissions, a complete allocation to the output flows can be determined. Consequently, the methods can be expected to be transferable to heat pumps.

3.6.3. Exergy method

To apply the ExM to HPs, it is necessary to evaluate two thermal energy flows exergetically. For this purpose, the logarithmic temperature values for the primary side $T_{m,prim,j}(t)$ and secondary side $T_{m,sec,j}(t)$

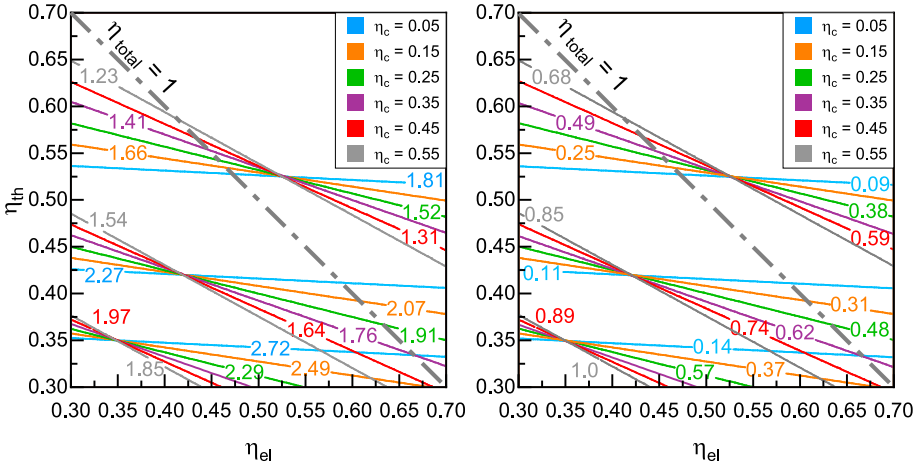

Fig. 8. Illustration of the allocation factors of the exergy method (ExM) for CHP: allocation factor electricity (left), allocation factor heat (right).

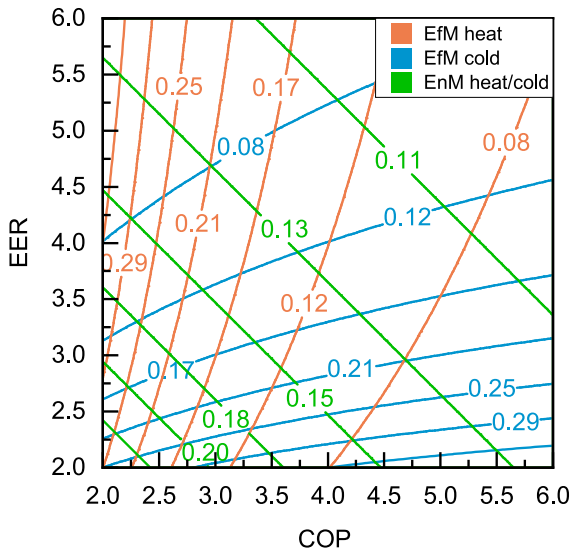

Fig. 9. Illustration of the allocation factors of the energy method (EnM) and efficiency method (EfM) for HPs.

are calculated from the measured values of the flow temperatures $T_{out,prim,j}(t), T_{out,sec,j}(t)$ and return temperatures $T_{in,prim,j}(t), T_{in,sec,j}(t)$:

$$T_{m,sec,j}(t) = \frac{T_{out,sec,j}(t) - T_{in,sec,j}(t)}{\ln \frac{T_{out,sec,j}(t)}{T_{in,sec,j}(t)}} \tag{24}$$

$$T_{m,prim,j}(t) = \frac{T_{in,prim,j}(t) - T_{out,prim,j}(t)}{\ln \frac{T_{in,prim,j}(t)}{T_{out,prim,j}(t)}} \tag{25}$$

In comparison with the ambient temperature, a Carnot efficiency can be derived for the secondary side $\eta_{C,sec,j}(t)$ and for the primary side $\eta_{C,prim,j}(t)$:

$$\eta_{C,sec,j}(t) = 1 - \frac{T_a(t)}{T_{m,sec,j}(t)} \tag{26}$$

$$\eta_{C,prim,j}(t) = \frac{T_a(t)}{T_{m,prim,j}(t)} - 1 \tag{27}$$

If equations (16) and (17) of [18] are adapted and a second Carnot factor is added, the exergetic emission allocation for HPs is as follows:

$$e_{sec,j}(t) = \frac{e_{in,j}(t) \frac{\eta_{C,sec,j}(t) COP_j(t)}{\eta_{C,sec,j}(t) COP_j(t) + \eta_{C,prim,j}(t) EER_j(t)} W_{in,j}(t)}{W_{out,sec,j}(t)} \tag{28}$$

$$e_{prim,j}(t) = \frac{e_{in,j}(t) \frac{\eta_{C,prim,j}(t) EER_j(t)}{\eta_{C,sec,j}(t) COP_j(t) + \eta_{C,prim,j}(t) EER_j(t)} W_{in,j}(t)}{W_{out,prim,j}(t)} \tag{29}$$

It is also possible to obtain a ratio $r_j(t)$ of the two Carnot efficiencies. This can be used to convert the equations (28) and (29) to the equations (31) and (32):

$$r_j(t) = \frac{\eta_{C,sec,j}(t)}{\eta_{C,prim,j}(t))} = \frac{(T_{m,sec,j}(t) - T_a(t)) T_{m,prim,j}(t)}{T_{m,sec,j}(t)(T_a(t) - T_{m,prim,j}(t))} \tag{30}$$

$$e_{sec,j}(t) = \frac{e_{in,j}(t) \frac{r_j(t) COP_j(t)}{r_j(t) COP_j(t) + EER_j(t)} W_{in,j}(t)}{W_{out,sec,j}(t)} \tag{31}$$

$$e_{prim,j}(t) = \frac{e_{in,j}(t) \frac{EER_j(t)}{r_j(t) COP_j(t) + EER_j(t)} W_{in,j}(t)}{W_{out,prim,j}(t)} \tag{32}$$

Using this ratio in a selected value range, the ExM for HPs can be represented as an illustration, see Fig. 10. The heat allocation factors are shown on the left and the cooling allocation factors are shown on the right.

3.7. Suggestion for a further and specific allocation method for hybrid HPs called the Bayreuth method (BaM)

The subsequent proposal delineates a new developed methodology, exclusively prepared for hybrid HPs providing heat and cold. This also implies that the BaM can be applied to chillers that utilize waste heat. The method entails a comparison of the output flows, alongside the efficiency or entropy generation of the cycle process. Consequently, the distribution of emissions is contingent not only on the exergy content of the thermal output flows, such as the ExM, but also on the internal exergetic efficiency for the heating and cooling supply. This procedure facilitates a more uniform distribution of emissions, as illustrated schematically in Fig. 11.

In the following method description, the Carnot factors of the output flows are defined as external exergetic efficiencies $\eta_{exe,sec,j}(t)$ and $\eta_{exe,prim,j}(t)$:

$$\eta_{exe,sec,j}(t) = \eta_{C,sec,j}(t) \tag{33}$$

$$\eta_{exe,prim,j}(t) = \eta_{C,prim,j}(t) \tag{34}$$

For this purpose, the reversible coefficient of performance $COP_{C,j}(t)$ and the reversible energy efficiency ratio $EER_{C,j}(t)$ are calculated:

$$COP_{C,j}(t) = \frac{T_{m,sec,j}(t)}{T_{m,sec,j}(t) - T_{m,prim,j}(t)} \tag{35}$$

$$EER_{C,j}(t) = \frac{T_{m,prim,j}(t)}{T_{m,sec,j}(t) - T_{m,prim,j}(t)} \tag{36}$$

The reversible performance factors of the system are set in relation to the real or measured performance factors. This gives the internal exergetic efficiency for the provision of heat $\eta_{exi,sec,j}(t)$ and for the provision of cooling $\eta_{exi,prim,j}(t)$:

$$\eta_{exi,sec,j}(t) = \frac{COP_j(t)}{COP_{C,j}(t)} \tag{37}$$

$$\eta_{exi,prim,j}(t) = \frac{EER_j(t)}{EER_{C,j}(t)} \tag{38}$$

These values can be used to extend the ratio defined in the ExM in Section 3.5.3:

$$r_j(t) = \frac{\eta_{exi,sec,j}(t)\eta_{exe,sec,j}(t)}{\eta_{exi,prim,j}(t)\eta_{exe,prim,j}(t)} = \frac{COP_j(t)\left(T_{m,sec,j}(t) - T_a(t)\right)T_{m,prim,j}(t)^2}{EER_j(t)(T_a(t) - T_{m,sec,j}(t))T_{m,sec,j}(t)^2} \tag{39}$$

The allocation of specific emissions can be achieved through the utilization of equation (31) and (32). The allocation factors also remain as shown in Fig. 10.

3.8. Energy storage

If an energy storage system is involved in the energy supply, emissions can be added to the supply grid with a temporal delay. The magnitude of these emissions is contingent on the timing and configuration of the charging of the storage system. As the emissions balance is calculated annually and the storage status at the turn of the year is unknown, only the emissions absorbed by the storage in the year examined are included. To visualize the course of the emissions released, it is first necessary to calculate the energy status $C_j(t)$ of the storage. The initial value is assumed to be $C_j(0) = 0$:

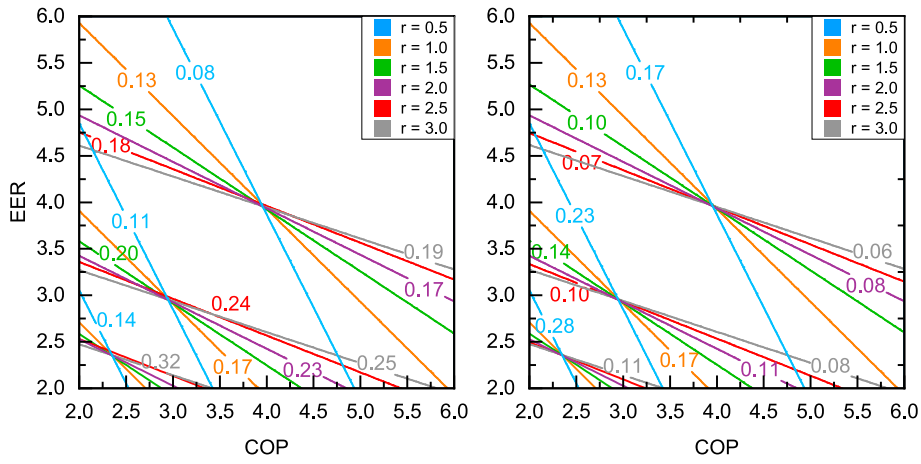

Fig. 10. Illustration of the allocation factors of the exergy method (ExM) for heat pumps: allocation factor heat (left) and allocation factor cold (right).

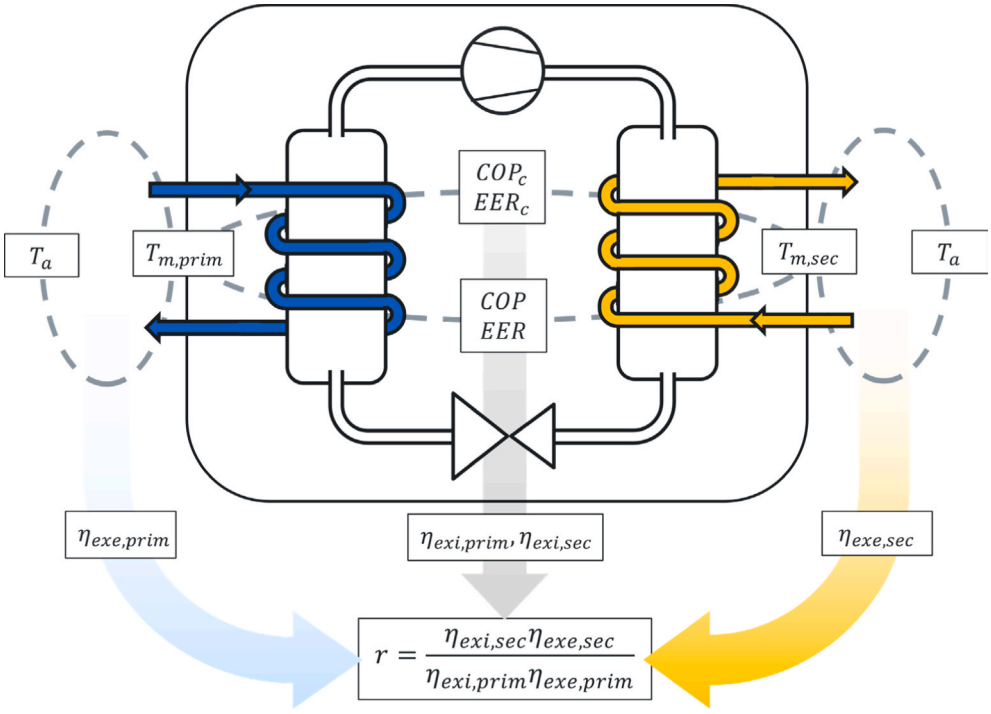

Fig. 11. Schematic representation of the Bayreuth method (BaM).

$$C_j(t) = C_j(t-1) + W_{ij}(t) - W_{jk}(t) \tag{40}$$

This calculation is based on the assumption that the storage condition cannot become negative. The condition curve is therefore shifted by the minimum $C_{min,j}$, resulting in a corrected condition curve $C_{corr,j}$:

$$C_{min,j} = \min_{t\in\{1,2,\cdots,8760\}} C_j(t) \tag{41}$$

$$C_{corr,j}(t) = C_j(t) - C_{min,j} \tag{42}$$

To obtain an initial status value of the emission load, the average emission load $e_{m,j}$ of the energy emitted is calculated. This is achieved by dividing the annual emissions absorbed by the energy released:

$$e_{m,j} = \frac{\sum_{t=1}^{H}\sum_i W_{ij}(t)e_{ij}(t)}{\sum_{t=1}^{H}\sum_k W_{jk}(t)} \tag{43}$$

Now it is possible to estimate an initial amount of stored emissions. This is derived from the energy condition and the average emissions load:

$$E_j(0) = C_{corr,j}(0)e_{m,j} \tag{44}$$

$$e_{jk}(0) = e_{m,j} \tag{45}$$

The quantity of stored emissions is determined for each point in time based on this initial value:

$$E_j(t) = E_j(t-1) + W_{ij}(t)e_{ij}(t) - W_{jk}(t)e_{jk}(t-1) \tag{46}$$

By comparing this with the energy status of the storage, specific emission values can be calculated:

$$e_{jk}(t) = \frac{E_j(t)}{C_{corr,j}(t)} \tag{47}$$

Once this curve of specific emissions has been approximated, the posi-

tion of the curve is customized using a balance adjustment (see Section 3.9). In this way, the losses of the storage systems can also be considered.

3.9. Balance adjustment

The various energy readings are sometimes recorded with a time lag due to the different measurement systems. In addition, there are measurement uncertainties and losses between and within the systems, which can lead to an increase in the specific emissions and thus to a discrepancy. To ensure that the imported emissions are fully allocated, a balance correction is performed at each node. This is based on Kirchhoff's nodal rule. The underlying principle is that the sum of all annual input flows must equal to the sum of all annual output flows:

$$\sum_{t=1}^{H}\sum_{i}W_{ij}(t)e_{ij}(t)=\sum_{t=1}^{H}\sum_{k}W_{jk}(t)e_{jk}(t) \tag{48}$$

On this basis, a correction factor $corr_j$ is calculated by comparing the input and output flows:

$$corr_j=\frac{\sum_{t=1}^{H}\sum_{i}W_{ij}(t)e_{ij}(t)}{\sum_{t=1}^{H}\sum_{k}W_{jk}(t)e_{jk}(t)} \tag{49}$$

This correction factor is used to make an adjustment to the specific emissions that emanate from the node:

$$e_{corr,jk}(t)=corr_j e_{jk}(t) \tag{50}$$

4. Results and discussion

In the following section, the results of the allocation model are presented and the influence of temporal emission factors and allocation methods is analyzed. Furthermore, the implementation and evaluation of the BaM is carried out.

4.1. Results of the dynamic accounting model

According to the described methodology it is possible to transfer input values to the model. These flows are tracked and allocated through the entire model and finally retrieved at the output nodes. In this way, a specific emission value can be calculated for the energy grids for every hour of the year. However, it should be noted that the evolution of these values depends on the resolution at which the input emissions load from the public electricity grid is entered and the allocation method chosen for the CHP and HP. For a better comparability, the same allocation method is always used for these two systems. To observe the effects of these factors for the year 2023, the cumulative annual emission amounts

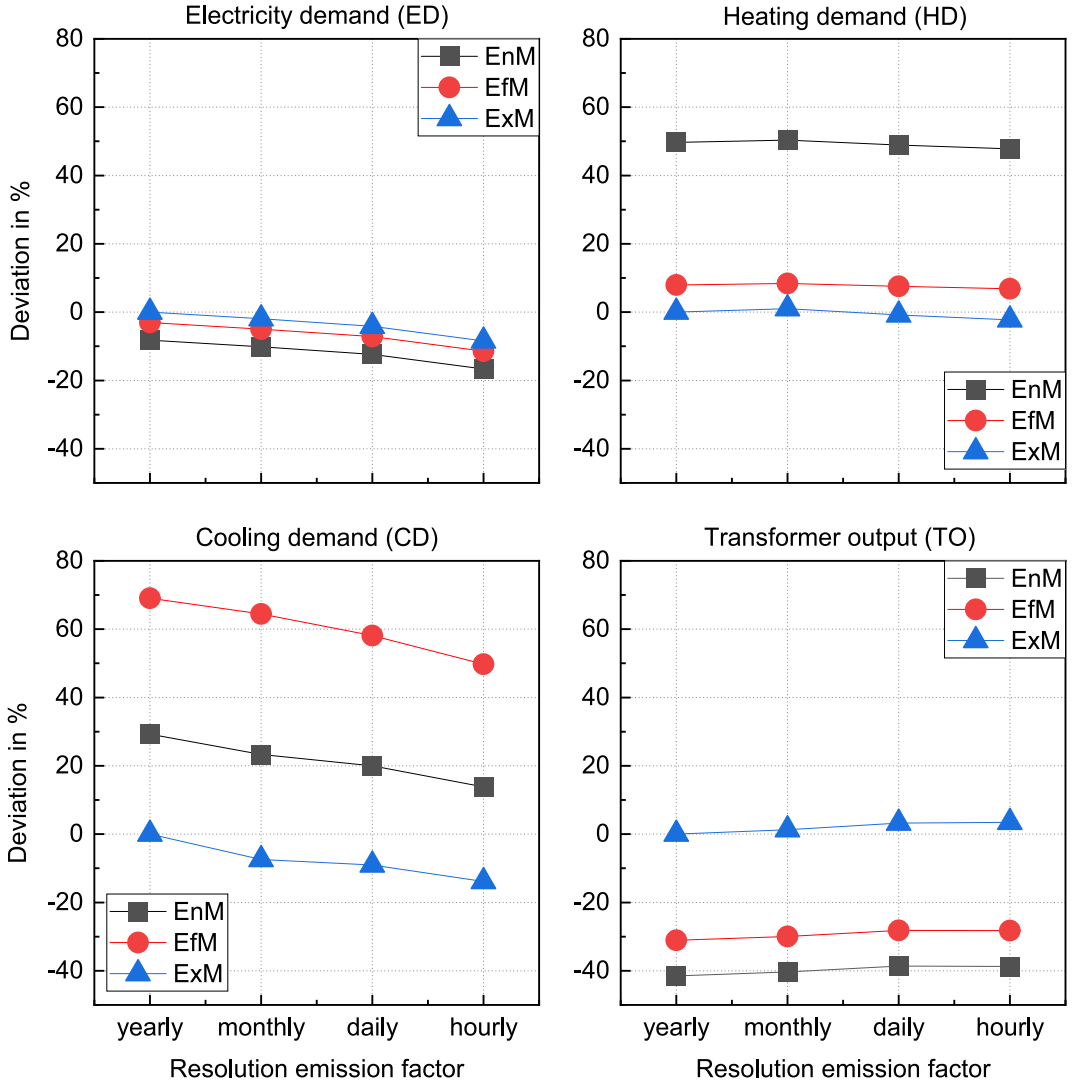

Fig. 12. Deviation between the cumulative emissions of 2023 at the output nodes as a function of the resolution of purchased emission loads from the public electricity grid and different allocation methods for the CHP and the HP, with reference to the exergy method (ExM) with a yearly resolution.

at the output nodes are calculated for every combination of allocation methods and emission load resolutions, see Fig. 22 in the Appendix. The relative deviations are shown in Fig. 12. For this purpose, the ExM with an annual emission factor is used as a reference point here.

As the allocation is contingent on the measured values, the methods may also vary at each time step. Nevertheless, the tendency of the examined methods is clearly visible in Fig. 12. The EnM depends on the overall efficiency and distributes the specific emissions evenly across the output flows. In this case, the distribution is consequently determined by the varying demand quantities. The EfM, on the other hand, compares the two partial efficiencies and allocates a greater proportion of emissions to the less efficient part. As illustrated by HD and CD, a bigger amount of emissions is attributed to the cooling energy. The significance of the ExM becomes particularly evident when examining ED, HD and CD. If the CHP unit is considered separately, the allocation is predominantly made to the electrical energy. This is attributable to the higher exergy content.

In addition to the allocation methods, the emission balance is also influenced by the resolution of the emission factors. This dependency is especially visible in the cumulative values of the purchased electricity, see ED. The effect observed here is caused by the temporal course of the ED of the building. To further illuminate this phenomenon, Fig. 13 shows the curve for an example week in 2023.

Here it can be seen that the temporal distribution of the electricity consumption particularly benefits from hourly emission factors. An analysis of the mean value across the various methods reveals a discrepancy of approximately 47 tons CO_2-eq per year between an annual and an hourly resolution, as evidenced only by an analysis of the electricity grid. As the refrigeration systems are operated using electricity from the internal grid, this effect is as well as mitigated at the cooling grid, see CD. A similar relationship is evident in the heating grid, which is connected to the electricity grid via the HP. However, especially in winter a large part of the thermal energy is provided by the GB and CHP, so the effect is only weakly pronounced on the scale shown. In contrast to the three supply grids, the emissions recorded at the TO increase with higher resolution. This is caused by the way the CHP unit operates. When the CHP unit is running at night, the electricity produced cannot be completely used in the building, leading to its export to the public grid. At the onset of this transitional period, an overlap emerges between consumption and feed-in. The initiation of the CHP unit is incapable of providing the entire electricity demand, resulting in a proportion of the required load drawn from the public grid.

Assuming the building structure under consideration is designated as the balance boundary and exclusively considering emission flows, the emissions caused by the energy grids can be attributed to the TAO building. Conversely, the emissions released to the public grid are not factored in this analysis. This results in total values of between 614 and 670 tons of CO_2-eq for the year 2023.

As part of a comparison with previous studies, it is possible to compare the sum of resulting emissions of the HD and CD with the current values. In this context, Griesbach et al. [25] analyze various operating strategies with regard to the IES. An annual analysis between the years 2020 und 2021 results in a range of 148 and 235 tons of CO_2-eq. The dynamic accounting model presented here results in values between 104 and 158 tons of CO_2-eq. It is evident that the value ranges overlap, although it should be noted that these are different reference years.

As an example for the dynamic emission loads, Fig. 14 shows the specific emissions of the three internal grids for the year 2023. The emission load of the electricity purchased from the public grid is selected here in a monthly resolution. The allocation is carried out using the EnM. To enhance the visual representation of the data, the curves have been filtered using the moving average.

The monthly trend in the emission load of the TAO electricity grid is clearly visible. During the winter months, the CHP unit also influences the specific emissions of the electricity grid. As the output of the installed PV system accounts for a small proportion of the ED, only a minor influence can be observed in the summer months. In the case of the heating grid, the average emission load is higher in the winter months than in the summer months, which is due to the operation of the GB and the CHP. During the summer, the HD can largely be covered by the HP, resulting in relatively low emissions during this period. In the reference year, the CD can be provided from the IES until the beginning of May. Consequently, the CC provides support, engendering an irregular emission load.

For the purpose of comparison, an hourly emission factor is specified for the model and allocated using the EnM, see Fig. 15. As can be observed here, the dynamics of the emission load from the public grid are transferred to the local grid of the TAO building. Due to the electricity consumption of the HP and CC, this also has an impact on the heating and cooling grid.

As a further example, an hourly emission factor is specified for the model and allocated using the ExM, see Fig. 16. A comparison of Fig. 15 with Fig. 16 demonstrates that the course and distribution of the emission curves are subject to alteration by the allocation methods. The analysis of the cooling grid, especially at the beginning of the year, shows that the emission load is lower. This is attributable to the exergy content of the HPs cooling output, which consequently leads to a lower quantity of emissions being charged to the IES. The ExM also has an impact on the heating grid, particularly through the allocation of the CHP. The significant difference in exergy between electricity and thermal energy results in a smaller allocation of emissions to the heating grid.

The present results demonstrate that the hourly emission factors of

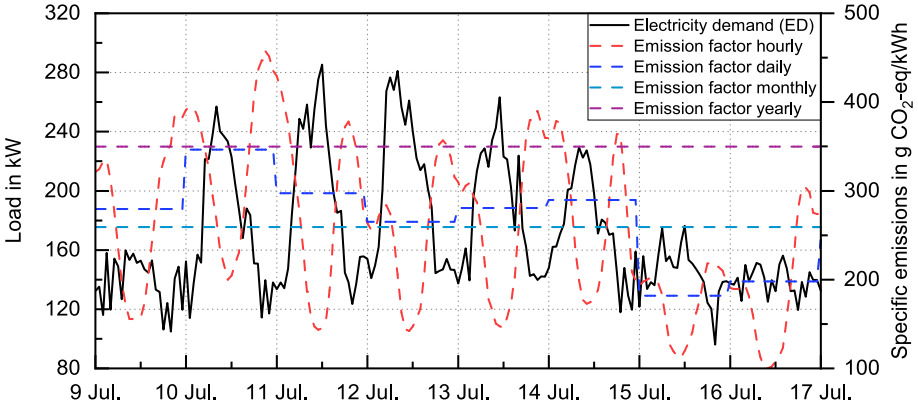

Fig. 13. Comparison between the electricity demand (ED) of the TAO building and the different resolutions of emission loads which are purchased from the public grid for an example summer week in 2023 with data from Electricity Maps [10].

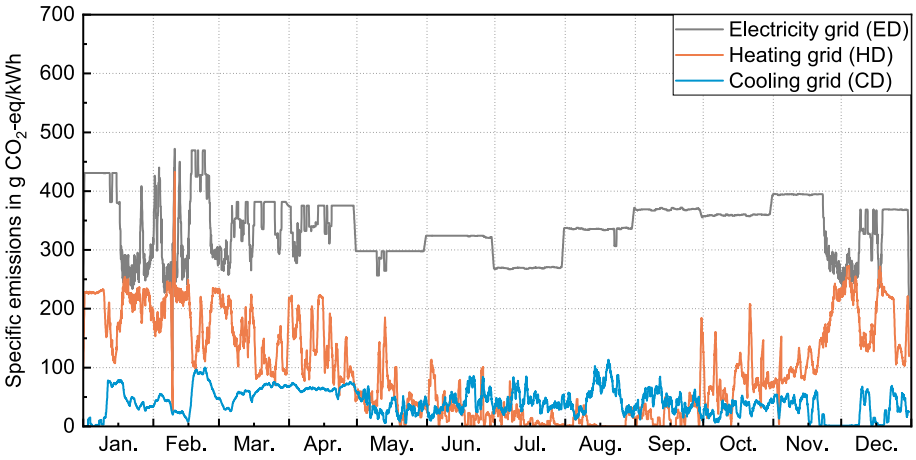

Fig. 14. Example emission loads of the supply grids for the year 2023; Allocation method for CHP and HP: energy method (EnM), resolution of emissions from the public electricity grid: monthly; reference nodes in the computational model: ED, HD and CD.

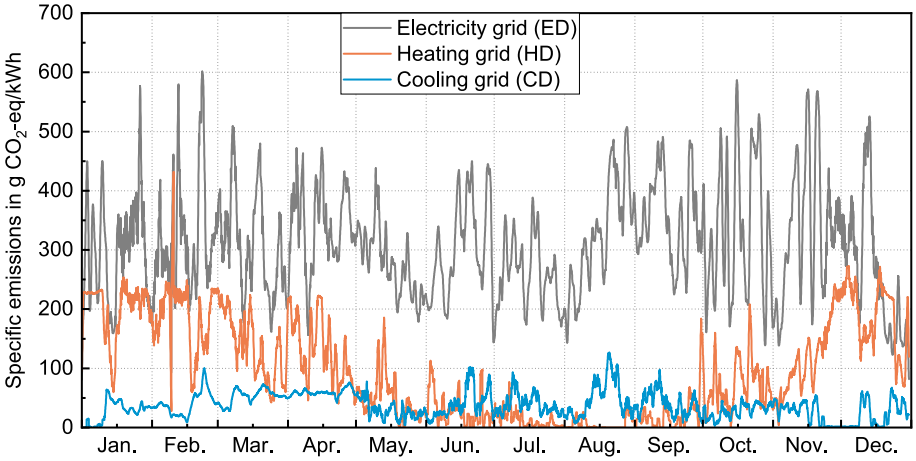

Fig. 15. Example emission loads of the supply grids for the year 2023; Allocation method for CHP and HP: energy method (EnM), resolution of emissions from the public electricity grid: hourly; reference nodes in the computational model: ED, HD and CD.

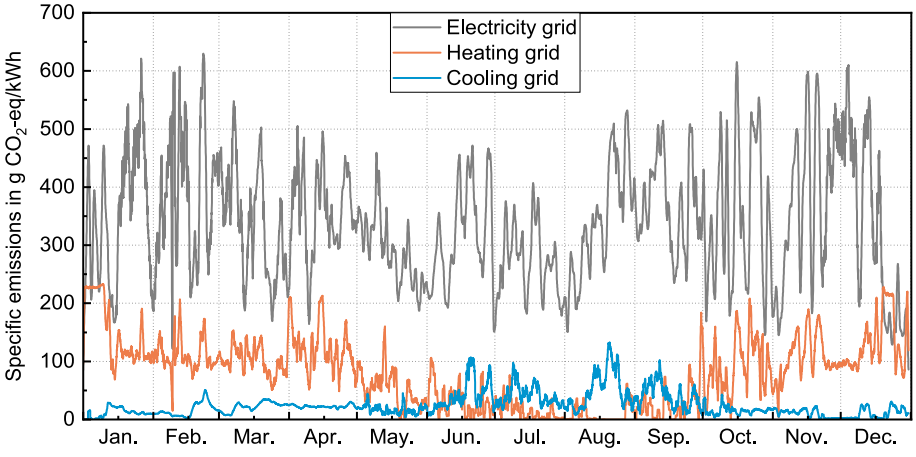

Fig. 16. Example emission loads of the supply grids for the year 2023; Allocation method for CHP and HP: exergy method (ExM), resolution of emissions from the public electricity grid: hourly; reference nodes in the computational model: ED, HD and CD.

the public electricity grid have the greatest dynamic influence on the internal supply grids. In order to facilitate a more robust comparison of the allocation methods and to provide a more effective illustration of the fluctuation ranges, the emission loads are presented in the form of ordered annual duration curves. As a comparison, the duration curve of the public electricity grid is also shown in an hourly resolution, see Fig. 17.

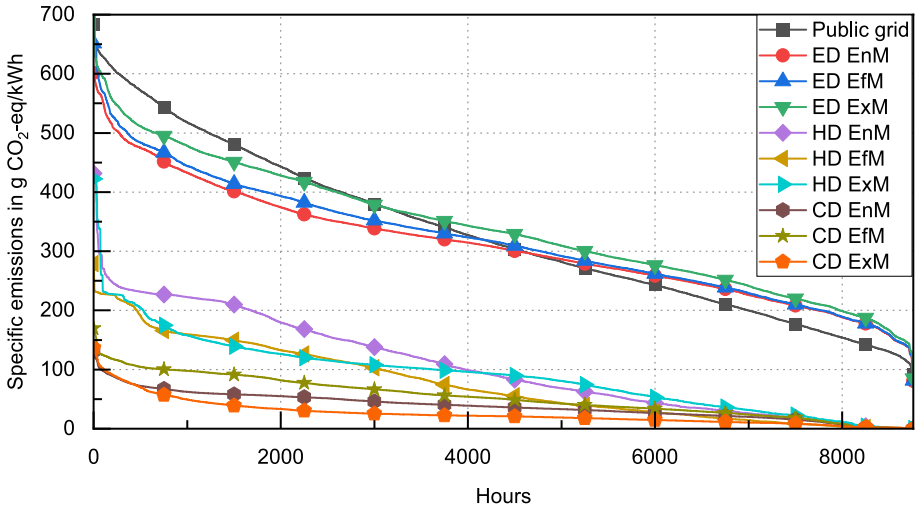

Fig. 17. Ordered annual duration curves of the emission loads of the electricity grid (ED), the heating grid (HD) and the cooling grid (CD) for the year 2023 depending on the allocation methods: energy method (EnM), efficiency method (EfM) and exergy method (ExM); resolution of emissions from the public electricity grid: hourly.

4.2. Implementation of the Bayreuth method (BaM)

The BaM, as outlined in Section 3.7, is in the following applied to the case study. As this is an extension of the ExM, it will serve as a comparison. This means that only the allocation method for the HP is changed; the method selected for the CHP remains constant and is also the ExM. The division of emissions therefore differs between the heating and cooling grid and can be attributed to the allocation method of the HP. To analyze the influence of BaM in detail, only the output flows of the HP are examined, as shown in Fig. 18. Here, too, the ExM with an annualized emission factor is used as a reference point.

In contrast to the pure ExM, the BaM also incorporates the reversibility of the circular process of the HP for the emission division. This signifies that the exergy content of the output flows with regard to the environment is not the sole consideration, but also the internal exergetic efficiency. A comparison of the distributions reveals that the BaM allocates a greater proportion of emissions to the refrigeration grid. In view of the available evidence, it can therefore be assumed that the provision of cooling by the HP implemented in this case study is on average more efficient than the provision of heat. An analysis of the effect caused solely by the allocation method shows that a difference of almost 15 % can be determined when considering the HP alone.

In this case, the heating and cooling supply of the whole building is not provided exclusively by the HP, which leads to small differences in the analysis of supply grids, see Fig. 23 in the Appendix. However, as the proportion of HP increases, the influence of the allocation method also rises. For this reason, it is imperative that the allocation method is accurate in its distribution of emissions across the output flows. This becomes particularly relevant if the emission flows exceed the balance limit and have to be distributed between different parties, like in district networks or municipal supply networks. The BaM should therefore determine the emissions as accurately as possible by taking a dual view of the system and supplementary its environment.

5. Conclusion

The present paper proposes a dynamic emission accounting model, predicated on a case study of a research building equipped with a decentralized energy system, which provides heating, cooling and electricity. In conjunction with other supply components and energy storages, this system incorporates a CHP and a hybrid HP, which is coupled with an IES. The interaction of these single-input/multiple-output components on the energy and emission-related exchange between the three supply grids is analyzed using a numerical QIO-model in

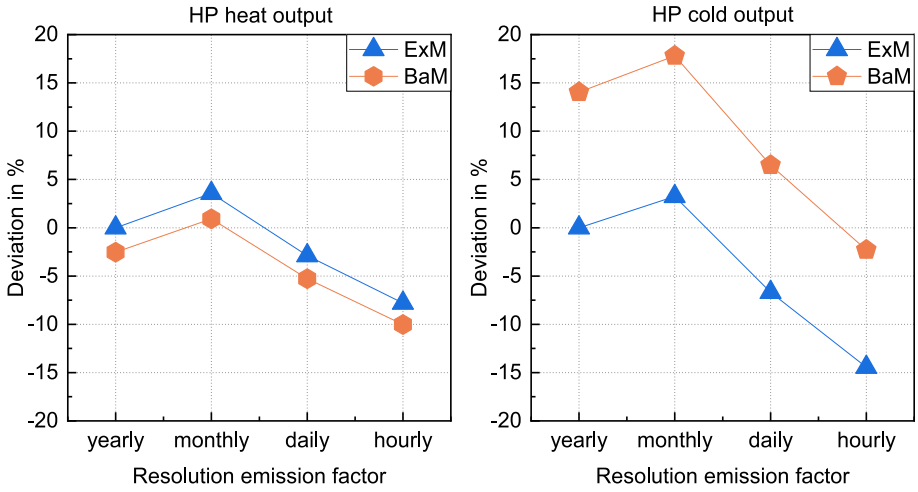

Fig. 18. Deviation between the cumulative emissions of 2023 at the HP output resulting from the exergy method (ExM) and Bayreuth method (BaM) as a function of different resolutions of purchased emission loads from the public electricity grid, with reference to the exergy method (ExM) with a yearly resolution.

Python. It is based on the emission flow theory and utilizes hourly-resolved measured values of the individual supply systems over the course of one year. The analysis encompasses two key aspects: the dynamics within the balance boundary, which is represented by the building envelope, and the dynamic behavior of the emission load of the electricity supply from the public grid. The temporal distribution of emissions is determined by the application of established CHP allocation methods. These methods are not only applied to the CHP, but also transferred to the HP. Additionally, an allocation method specifically for HPs is presented, referred to as the BaM.

The model is formulated as a node model, with different node types considering the properties of the installed components and mapping the structure of the system. Furthermore, various allocation methods have been incorporated, available for utilization by the designated nodes. For this purpose, the EnM, EfM and ExM were selected because they exclusively concern the system under consideration and do not involve comparisons with reference systems. This approach aims to ensure transferability to HPs and leads to the first result of this study. Consequently, the transferability and functionality of the EnM, EfM and ExM can be confirmed for HPs, with minor customizations. Moreover, the BaM can be integrated into the model, whereby a more even distribution between the heating and cooling grid can be observed. Compared to the ExM, the BaM allocates almost 15 % more emissions to the cooling energy of the HP. For the subsequent calculations of the whole system, the same method is consistently used in the model for the CHP and HP in order to ensure an equivalent distribution. This results in significant diverging emission ratios between the supply grids. Consequently, there are discrepancies of up to 70 % in annual emissions within the cooling grid. In addition, the total amount of the accounting result is influenced by the resolution of the emission factor of purchased electricity. An observation with the mean value of the allocation methods shows that there is a difference of 47 tons CO_2-eq per year between an annual and an hourly resolution focusing only on the electricity demand. This corresponds to around 8 %. The analysis of the overall balance within the balance limit, considering the effect of the allocation methods and the temporal resolution of the purchased electricity, results in a total quantity of emissions between 614 and 670 tons CO_2-eq for the year under review.

Due to the transferability of the model, the consideration of different load profiles and system combinations could be of interest for further investigations. The resulting emission profiles can be used not only for detailed emission calculations, but also for energy management strategies. This would also provide a decisive benefit for existing energy systems. With regard to the presented BaM, further investigations could be carried out to analyze the effects on different types of HPs, including their partial load behavior, as well as on chillers with heat recovery.

CRediT authorship contribution statement

Chris Burkel: Writing – review & editing, Writing – original draft, Visualization, Software, Formal analysis, Data curation, Conceptualization. **Marco Griesbach:** Writing – review & editing, Writing – original draft, Formal analysis, Data curation, Conceptualization. **Florian Heberle:** Writing – review & editing, Writing – original draft, Conceptualization. **Dieter Brüggemann:** Writing – review & editing, Writing – original draft, Supervision, Project administration. **Andreas Jess:** Writing – review & editing, Writing – original draft, Supervision, Project administration.

Declaration of competing interest

The authors declare that they have no known competing financial interests or personal relationships that could have appeared to influence the work reported in this paper.

Acknowledgments

The authors gratefully acknowledge the financial support of the Bavarian State Ministry of Education, Science and the Arts within the Research Training Group “Energy self-sufficient buildings” of the Technology Alliance Upper Franconia (TAO). Additionally, the authors gratefully acknowledge the financial support of the Upper Franconian Trust within the project “KomWEisS”.

Appendix

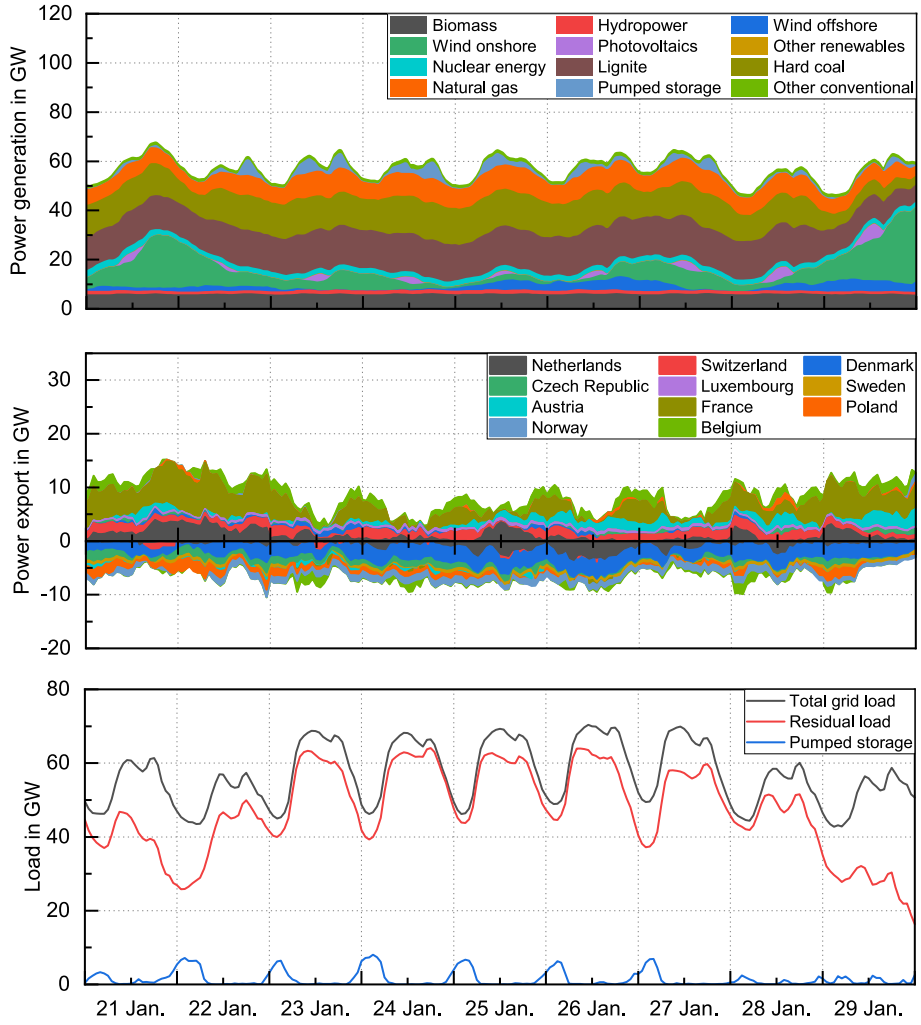

Fig. 19. Example winter week in 2023 of the German electricity production, the import/export behavior and the national electricity demand based on the data from SMARD [27].

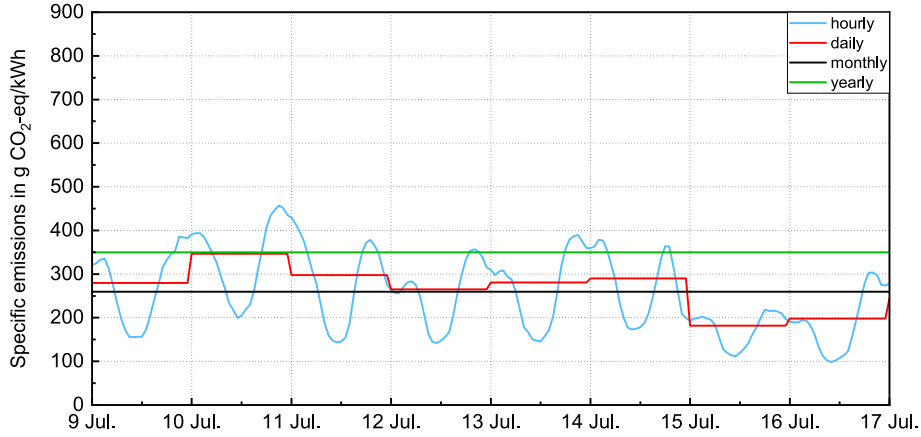

Fig. 20. Different resolutions of the emission load of the German public electricity grid for an example summer week for the year 2023 based on the data from Electricity Maps [10].

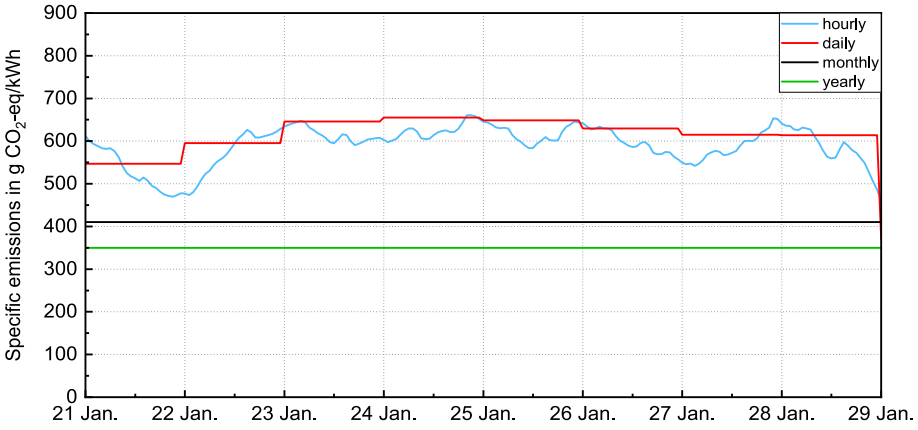

Fig. 21. Different resolutions of the emission load of the German public electricity grid for an example winter week for the year 2023 based on the data from Electricity Maps [10].

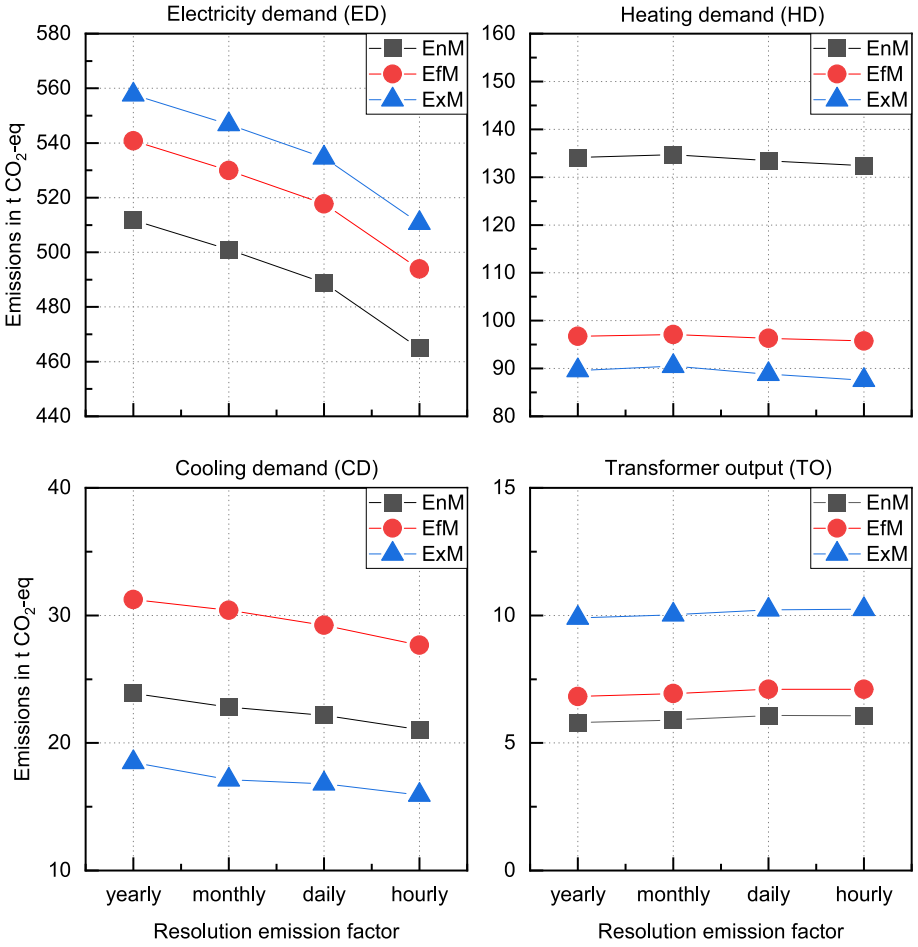

Fig. 22. Cumulative annual emissions of 2023 at the output nodes as a function of the resolution of purchased emission loads from the public electricity grid and different allocation methods for the CHP and the HP.

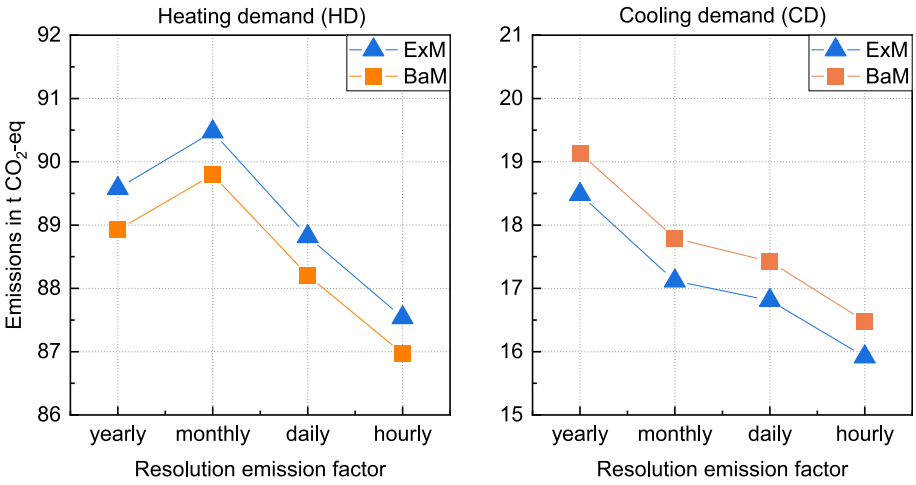

Fig. 23. Cumulative emissions amount for the HD and CD resulting from HP with the exergy method (ExM) and the Bayreuth method (BaM) as functions of different resolutions of purchased emission loads from the public electricity grid.

Data availability

Data will be made available on request.

References

[1] Umweltbundesamt. Treibhausgas-Projektionen 2024 – Ergebnisse kompakt. (in German); Available from: https://www.umweltbundesamt.de/publikationen/treibhausgas-projektionen-2024-ergebnisse-kompakt, Accessed 24.02.2025.

[2] Agora Energiewende. Energiewende und Dezentralität. Zu den Grundlagen einer politisierten Debatte. (in German); Available from: https://www.agora-energiewende.de/fileadmin/Projekte/2016/Dezentralitaet/Agora_Dezentralitaet_WEB.pdf, Accessed 24.02.2025.

[3] Khan I, Jack MW, Stephenson J. Analysis of greenhouse gas emissions in electricity systems using time-varying carbon intensity. J Clean Prod 2018;184:1091–101. https://doi.org/10.1016/j.jclepro.2018.02.309.

[4] Huang X, Jiang K, Luo S, Li H, Lu Z. Dynamic calculation method for zonal carbon emissions in power systems based on the theory of production simulation and carbon emission flow theory. Sustainability 2024;16(15):6483. https://doi.org/10.3390/su16156483.

[5] Qu S, Wang H, Liang S, Shapiro AM, Suh S, Sheldon S, et al. A Quasi-Input-output model to improve the estimation of emission factors for purchased electricity from interconnected grids. Appl Energy 2017;200:249–59. https://doi.org/10.1016/j.apenergy.2017.05.046.

[6] Röder J, Beier D, Meyer B, Nettelstroth J, Stührmann T, Zondervan E. Design of renewable and system-beneficial district heating systems using a dynamic emission factor for grid-sourced electricity. Energies 2020;13(3):619. https://doi.org/10.3390/en13030619.

[7] Li J, Zhou Z, Wen B, Zhang X, Wen M, Huang H, et al. Modeling and analysis method for carbon emission flow in integrated energy systems considering energy quality. Energy Sci Eng 2024;12(6):2405–25. https://doi.org/10.1002/ese3.1747.

[8] Li J, Zou N, Wu J, Yang Q. Low carbon optimal dispatching of power system considering carbon emission flow theory. In: 2022 9th International Forum on Electrical Engineering and Automation (IFEEA). IEEE; 2022, p. 532–536.

[9] Tranberg B, Corradi O, Lajoie B, Gibon T, Staffell I, Andresen GB. Real-time carbon accounting method for the European electricity markets. Energ Strat Rev 2019;26:100367. https://doi.org/10.1016/j.esr.2019.100367.

[10] Electricity Maps ApS. Electricity Maps; Available from: https://www.electricitymaps.com, Accessed 24.02.2025.

[11] World Business Council for Sustainable Development, World Resources Institute. The Greenhouse Gas Protocol: A Corporate Accounting and Reporting Standard; Available from: https://ghgprotocol.org, Accessed 24.02.2025.

[12] Bontekoe E, Schade J, Erikkson L, Tsarchopoulos P, Lampropoulos I, van Sark W. On the discrepancy of using annual or hourly emission factors for power generation to estimate CO2 reduction of building retrofitting. Energ Buildings 2024;319:114499. https://doi.org/10.1016/j.enbuild.2024.114499.

[13] He H, Zhou S, Zhang L, Zhao W, Xiao X. Dynamic Accounting Model and Method for Carbon Emissions on the Power Grid Side. Energies 2023;16(13):5016. https://doi.org/10.3390/en16135016.

[14] Roux C, Schalbart P, Peuportier B. Accounting for temporal variation of electricity production and consumption in the LCA of an energy-efficient house. J Clean Prod 2016;113:532–40. https://doi.org/10.1016/j.jclepro.2015.11.052.

[15] Álvarez Flórez L, Péan T, Salom J. Hourly based methods to assess carbon footprint flexibility and primary energy use in decarbonized buildings. Energ Build 2023;294:113213. https://doi.org/10.1016/j.enbuild.2023.113213.

[16] Chicco G, Mancarella P. Assessment of the greenhouse gas emissions from cogeneration and trigeneration systems. Part I: models and indicators. Energy 2008;33(3):410–7. DOI: 10.1016/j.energy.2007.10.006.

[17] Mancarella P, Chicco G. Assessment of the greenhouse gas emissions from cogeneration and trigeneration systems. Part II: Analysis techniques and application cases. Energy 2008;33(3):418–30. https://doi.org/10.1016/j.energy.2007.10.008.

[18] Buchenau N, Hannen C, Holzapfel P, Finkbeiner M, Hesselbach J. Allocation of carbon dioxide emissions to the by-products of combined heat and power plants: a methodological guidance. Renew Sustain Energy Transition 2023;4:100069. https://doi.org/10.1016/j.rset.2023.100069.

[19] Rosen MA. Allocating carbon dioxide emissions from cogeneration systems: descriptions of selected output-based methods. J Clean Prod 2008;16(2):171–7. https://doi.org/10.1016/j.jclepro.2006.08.025.

[20] Noussan M. Allocation factors in combined Heat and Power systems – Comparison of different methods in real applications. Energ Conver Manage 2018;173:516–26. https://doi.org/10.1016/j.enconman.2018.07.103.

[21] Holmberg H, Tuomaala M, Haikonen T, Ahtila P. Allocation of fuel costs and CO2-emissions to heat and power in an industrial CHP plant: Case integrated pulp and paper mill. Appl Energy 2012;93:614–23. https://doi.org/10.1016/j.apenergy.2011.11.040.

[22] Cheng Y, Zhang N, Wang Y, Yang J, Kang C, Xia Q. Modeling Carbon Emission Flow in Multiple Energy Systems. IEEE Trans Smart Grid 2019;10(4):3562–74. https://doi.org/10.1109/TSG.2018.2830775.

[23] Yang W, Huang Y, Zhang T, Zhao D. Mechanism and analytical methods for carbon emission-exergy flow distribution in heat-electricity integrated energy system. Appl Energy 2023;352:121980. https://doi.org/10.1016/j.apenergy.2023.121980.

[24] Griesbach M, König-Haagen A, Brüggemann D. Numerical analysis of a combined heat pump ice energy storage system without solar benefit – Analytical validation and comparison with long term experimental data over one year. Appl Therm Eng 2022;213:118696. https://doi.org/10.1016/j.applthermaleng.2022.118696.

[25] Griesbach M, König-Haagen A, Heberle F, Brüggemann D. Multi-criteria assessment and optimization of ice-energy storage systems in combined heat and cold supply networks of a campus building. Energ Conver Manage 2023;287:117118. https://doi.org/10.1016/j.enconman.2023.117118.

[26] Meteorological data at the Ecological Botanical Gardens, University of Bayreuth, from 2023 to 2023, Micrometeorology group, Prof. Dr. Thomas, BayCEER, University of Bayreuth, 2024.

[27] Bundesnetzagentur. SMARD. (in German); Available from: https://www.smard.de, Accessed 24.02.2025.

[28] European Network of Transmission System Operators for Electricity. ENTSO-E; Available from: https://www.entsoe.eu, Accessed 24.02.2025.

[29] Schlömer S., T. Bruckner, L. Fulton, E. Hertwich, A. McKinnon, D. Perczyk, J. Roy, R. Schaeffer, R. Sims, P. Smith, and R. Wiser, 2014: Annex III: Technology-specific cost and performance parameters. In: Climate Change 2014: Mitigation of Climate Change. Contribution of Working Group III to the Fifth Assessment Report of the Intergovernmental Panel on Climate Change [Edenhofer, O., R. Pichs-Madruga, Y. Sokona, E. Farahani, S. Kadner, K. Seyboth, A. Adler, I. Baum, S. Brunner, P. Eickemeier, B. Kriemann, J. Savolainen, S. Schlömer, C. von Stechow, T. Zwickel and J.C. Minx (eds.)]. Cambridge University Press, Cambridge, United Kingdom and New York, NY, USA.

[30] Raybaut P. Spyder IDE: The Scientific Python Development Environment. Spyder Project Contributors.

[31] Stadtwerke Bayreuth. Abrechnungsbrennwerte im Netzgebiet der Stadtwerke Bayreuth. (in German); Available from: https://www.stadtwerke-bayreuth.de/fileadmin/user_upload/netz/Netzzugang/Brennwertmatrix_01.pdf, Accessed 24.02.2025.